American Mineralogist, Volume 88, pages 18–26, 2003

Dissolution of gibbsite: Direct observations using fluid cell atomic force microscopy

CLAYTON D. PESKLEWAY,[1,*] GRANT S. HENDERSON,[1] AND FRED J. WICKS[2]

[1]Department of Geology, University of Toronto, 22 Russell Street Toronto, Ontario M5S 3B1, Canada
[2]Department of Earth Sciences, Royal Ontario Museum, 100 Queen's Park, Toronto, Ontario M5S 2C6, Canada

ABSTRACT

In situ atomic force microscopy (AFM) was used to follow the far-from-equilibrium dissolution of the {001} cleavage surface of natural gibbsite in nitric acid. The main dissolution mechanism was the retreat of straight monolayer steps, the edges of which are parallel to the <110>, <010>, and <100> directions. The stability of these steps can be expressed as <110> > <010> > <100>. The results are explained in terms of the positions of the terminal O atoms and their associated Al atoms at the steps. New steps were formed at etch pits that opened where screw dislocations emerged on the surface. The dissolution rates were calculated from the change in size of pits and islands. The values obtained were $9.5 \times 10^{-9} - 2.3 \times 10^{-8}$ mol/m^2·s, normalized to the total surface area, and $1.8 - 3.6 \times 10^{-7}$ mol/m^2·s, normalized to the surface area of the step fronts. The rates of dissolution calculated using only the surface area of the step fronts are similar to literature values obtained by other methods.

INTRODUCTION

The dissolution and growth of gibbsite [γ-Al(OH)$_3$] is an important process in the regulation of Al in natural waters (Lindsay and Walthall 1996), and in the industrial production of Al (Hind et al. 1999). Many quantitative studies have been carried out based on the dissolution of bulk quantities of gibbsite (e.g., Bloom 1983; Wesolowski and Palmer 1994; Mogollon et al. 1996). However, dissolution studies using microscopy are lacking, with only a few limited observations of dissolved gibbsite surfaces having been reported. Brown (1972), using SEM, observed large etch pits (~300 nm wide and of similar depth) on gibbsite grains dissolved in sodium hydroxide solutions, and Nagy and Lasaga (1992), also using SEM, observed large etch pits (on the scale of micrometers) on only a few of the microscopic grains of a gibbsite sample they had dissolved in nitric acid at pH 3.

In our study, the dissolution of gibbsite in nitric acid was observed in situ at the sub-micrometer scale using atomic force microscopy (AFM) in order to better determine the mechanism of gibbsite dissolution. AFM has been used previously to make in situ observations of changes in surface topography to explore the factors controlling mineral dissolution (e.g., Shindo and Nozoye 1993; Maurice et al. 1995). More recently, AFM has been used to quantify changes in surface features and to estimate the rates of dissolution (e.g., Jordan et al. 1999; Rufe and Hochella 1999; Bosbach et al. 2000; Shiraki et al. 2000).

Nitric acid is useful for a study of gibbsite dissolution in acidic conditions as it is common in nature (Mogollon et al. 1994), and the nitrate ion does not show evidence of direct participation in the gibbsite dissolution process (Bloom 1983; Bloom and Erich 1987). The pH of –0.9 used in our experiments represents far-from-equilibrium conditions for gibbsite with respect to the solution. However, far-from-equilibrium conditions have been observed in nature (Mulder et al. 1987; Wesselink et al. 1996), and may be applicable to many natural systems (Mogollon et al. 1996).

Gibbsite has perfect {001} cleavage, and the largest faces of gibbsite crystals are commonly {001} faces (Anthony et al. 1997). Therefore, this face accounts for most of the surface area of gibbsite. Steps on the {001} surfaces and other irregularities allow dissolution to take place in directions orthogonal to the [001] direction. We observed the changes in microtopography that occur with dissolution on this face and calculated the dissolution rates, normalizing them to both the surface area of the step fronts and the total surface area ({001} surfaces and surfaces of the step fronts combined).

EXPERIMENTAL METHODS

Gibbsite is monoclinic with the space group $P2_1/n$. The basic structural unit of gibbsite is a layer consisting of two sheets of closely packed hydroxyls with a central plane of Al atoms in the octahedral sites (Megaw 1934). These unit layers are oriented parallel to (001). A second layer overlies the first, and is offset slightly along the **a**-axis to produce the monoclinic structure. Successive layers are bonded together by H-bonding. For most experiments, a gibbsite from Vishnevye Gory, Ural Mountains, Russia was used, which occurs as crystals up to 3 mm in diameter in open spaces in the host rock. No grinding was required to break the crystals; the crystals and crystal fragments

* E-mail: clayton@galena.geology.utoronto.ca

0003-004X/03/0001–18$05.00

had mirror-flat {001} cleavage or crystal surfaces and were completely transparent. Both {100} and {110} faces were also observed. A second sample of botryoidal gibbsite from Hargreaves, Minas Gerais, Brazil (Royal Ontario Museum catalog number M 11980) was also used. A surface made up of {001} faces that was freshly exposed by light hammer taps was examined by AFM. The identity of the samples was confirmed by X-ray diffraction. Electron microprobe analyses indicated that both gibbsite samples contain (all values in wt%): <0.07 Fe_2O_3; <0.06 MnO; <0.04 ZnO; <0.03 CaO; <0.02 Na_2O, MgO, TiO_2 and Ga_2O_3; and <0.01 Cr_2O_3 and K_2O. The analyses also showed <0.10 wt% SiO_2 for the Russian gibbsite and ~0.16 wt% for the Brazilian gibbsite. The low levels of impurities, especially in the Russian gibbsite, make it probable that impurities did not significantly affect the dissolution process or the measured rates of dissolution, and that the rates at the nanometer scale observed using AFM were representative of the crystals as a whole.

Atomic force microscopy was performed with a Digital Instruments (DI) Nanoscope IIIa AFM operating in contact mode using standard DI square pyramidal silicon nitride (Si_3N_4) tips on V-shaped cantilevers 200 µm in length with 0.06 or 0.12 N/m spring constants. Samples 1–3 mm in diameter were mounted onto acid-resistant steel sample disks by means of a layer of epoxy. The DI fluid cell with a volume of 0.5 cm^3 was used. Height and deflection images were obtained simultaneously, and no filtering or other modification of the images was done.

In situ dissolution experiments with AFM require that the dissolution rate is not too slow or too fast in order to follow the changes in morphology within a reasonable period of time. Dove and Platt (1996) estimated that the dissolution rate for any sample under investigation should be 10^{-10} to 10^{-6} mol/m^2·s. In our experiments, because of the relative insolubility of gibbsite except in very acidic or basic conditions (Wefers and Misra 1987), an 8 *M* HNO_3 solution, corresponding to a pH of –0.9, was used to produce observable gibbsite dissolution. The solutions were made from reagent grade nitric acid and ultrapure deionized water.

A static fluid assembly was considered satisfactory for our experiments, because bulk studies of gibbsite dissolution in acidic conditions have demonstrated a large activation energy for dissolution (Bloom 1983) and dissolution rates independent of solution flow (Ganor et al. 1999); both these factors indicate that bulk diffusion generally would not be a significant factor in controlling the rate of gibbsite dissolution. Moreover, the low pH and small sample size in relation to the amount of fluid used, as well as the relatively short times for the experiments, were factors that favored minimal local gradients in the solution and ensured no back reaction. It was therefore assumed that the dissolution rate was constant during the course of an experiment; this assumption was supported by our measurements of step retreat and calculations of dissolution rates, both of which showed no significant changes with time. The physically stable, static fluid cell assembly also provided better stability between the tip and sample during the AFM experiments than would have been the case for a flow-through assembly. All experiments were carried out at room temperature, with an estimated fluid cell temperature of 20–24 °C based on literature experiments of heating due to the AFM laser (Dove and Chermak 1994; Kipp et al. 1995).

To assess the possible effect of tip/surface interactions on the dissolution process, the rate of dissolution was measured in intervals during which scanning took place and in intervals during which no scanning took place. No significant difference was found in the amount of dissolution observed. Moreover, in cases in which scanning causes mechanical degradation of the surface, surface features are aligned with the scanning direction (Maurice et al. 1995), but this was not observed. Also, during the course of the dissolution experiments, no significant changes in the surface roughness were evident as measured using the DI software. These results all indicate that the tip did not affect dissolution and that dissolution was due solely to the effect of the nitric acid on the surface.

In high-resolution images of the Russian gibbsite, the straight edges and uniform directionality of the features showed that no accumulation of surface fines, or mechanical disturbance of the surface, took place prior to imaging. Also, no globular, poorly ordered surface material, similar to that observed by Bloom and Weaver (1982) on the surfaces of synthetic gibbsite, was seen. In lower resolution scans of the Brazilian gibbsite some features appeared rounded, but the constancy of angles of the edges of the features indicated that most of the observed features represented the actual surface of the mineral; the apparent rounding was due largely to the lower resolution of the scans.

RESULTS

The AFM images show a series of straight-edged steps on the {001} surfaces of both the Brazilian and Russian gibbsite. The images of the Brazilian gibbsite show only the major steps (Fig. 1, an approximately 3000 by 3000 nm view), whereas those of the Russian gibbsite show the smallest steps and minor surface details (Fig. 2, an approximately 420 by 420 nm view). The higher resolution images of the Russian gibbsite (Fig. 2) show that the surface is characterized by pits approximately 30–100 nm in diameter separated by elevated areas, but the total vertical range is only 6–10 nm. Most of the linear edges of the surface features correlate with specific crystallographic directions.

In the images of the Brazilian gibbsite, and in the higher resolution images of the Russian gibbsite, three sets of steps on the surface correspond to three sets of crystallographic directions. In order to identify these directions, 18 and 55 angular measurements were made between the three sets of steps on the Brazilian and Russian gibbsite, respectively. The angles between the three step directions were found to be 60 and 90° for both samples. In both cases, the identification of crystal face edges at lower magnifications allowed us to index the step directions. For the Brazilian gibbsite, these were two <110> directions and a <130> direction, whereas for the Russian gibbsite, they were <110>, <010>, and <100>. These directions are indicated on Figures 1 and 2.

On the surface of the Russian gibbsite, an angle of 50° was measured (11 measurements) between the <010> steps and a fourth set of steps, which are shorter, less prominent and apparently non-crystallographic in orientation (Fig. 2, Table 1).

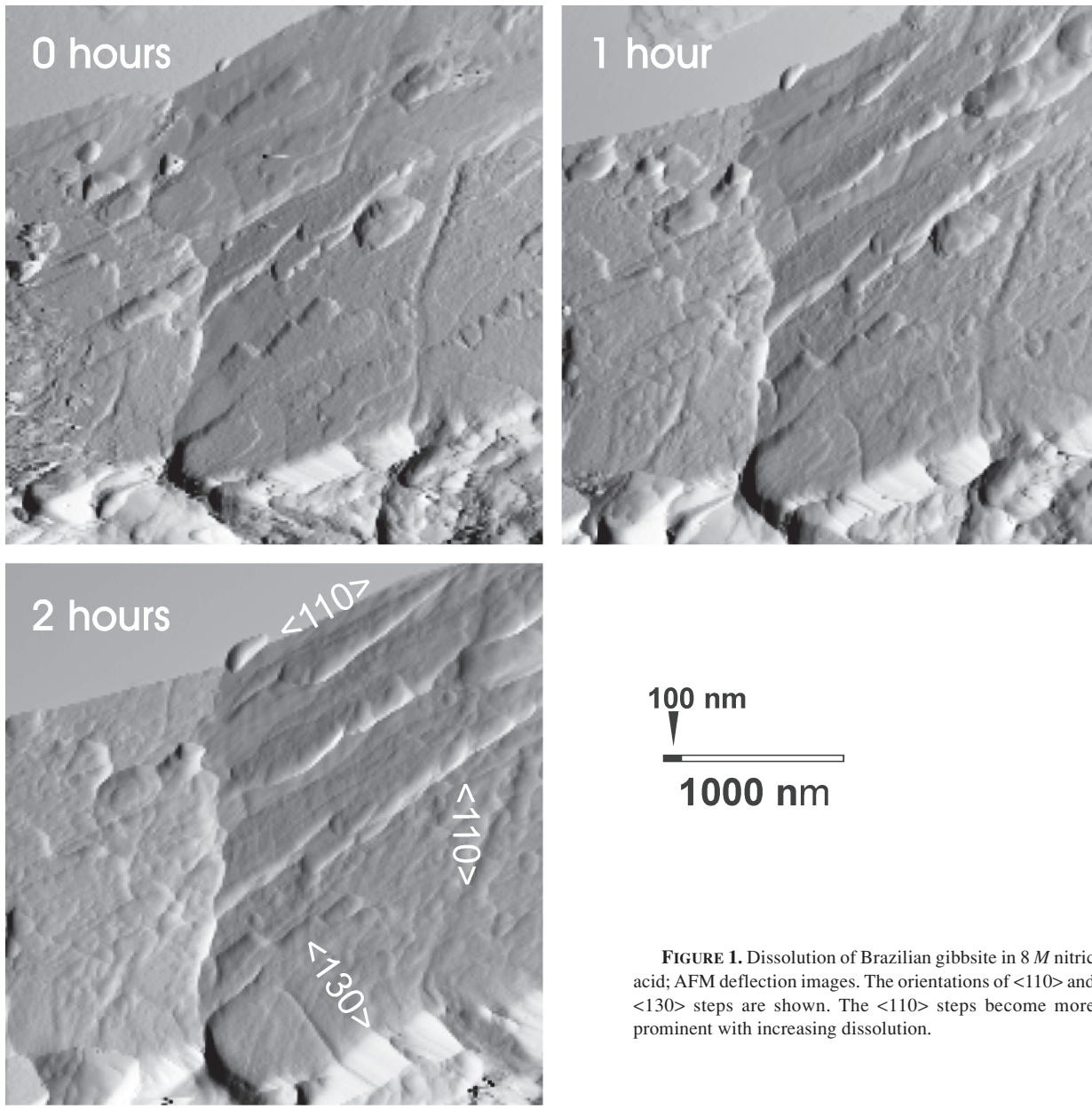

FIGURE 1. Dissolution of Brazilian gibbsite in 8 *M* nitric acid; AFM deflection images. The orientations of <110> and <130> steps are shown. The <110> steps become more prominent with increasing dissolution.

These steps appear to be cleavage steps, which are steps formed parallel to the cleavage direction, in this case from the top to the bottom of the images. In many cases, the terminations of these steps nearest the top of the images are points on the <001> surface, indicating that the steps were formed at the emergence points of screw dislocations. During the initial cleavage of the sample, the propagating steps commonly changed direction from the non-crystallographic direction of the cleavage steps to a more rational direction; this direction in most cases was <100>, probably because this direction is the closest to the cleavage direction. The change in direction of step propagation during the initial cleavage resulted in the formation of the shallow polygonal pits characteristic of the surface. The pits are initially bound by the <110>, <010>, and <100> steps and by cleavage steps of the non-crystallographic direction. The fact that the original {001} cleavage surfaces were characterized by steps of different crystallographic orientations and shallow pits rather than cleavage steps alone can be attributed to the perfect cleavage of gibbsite; the lack of force required to cleave the mineral allows low velocities of cleavage-surface propagation and therefore a greater likelihood of propagating steps changing direction to crystallographically favorable directions during cleavage.

In the images of the Russian gibbsite (Fig. 2), no marked difference was found in the step heights for the three crystallographic step directions (Table 1). The measured step heights were in the range $0.36 \pm 0.15 - 0.64 \pm 0.20$ nm. The thickness of a single $Al(OH)_3$ unit layer along [001] is 0.487 nm (Saalfeld

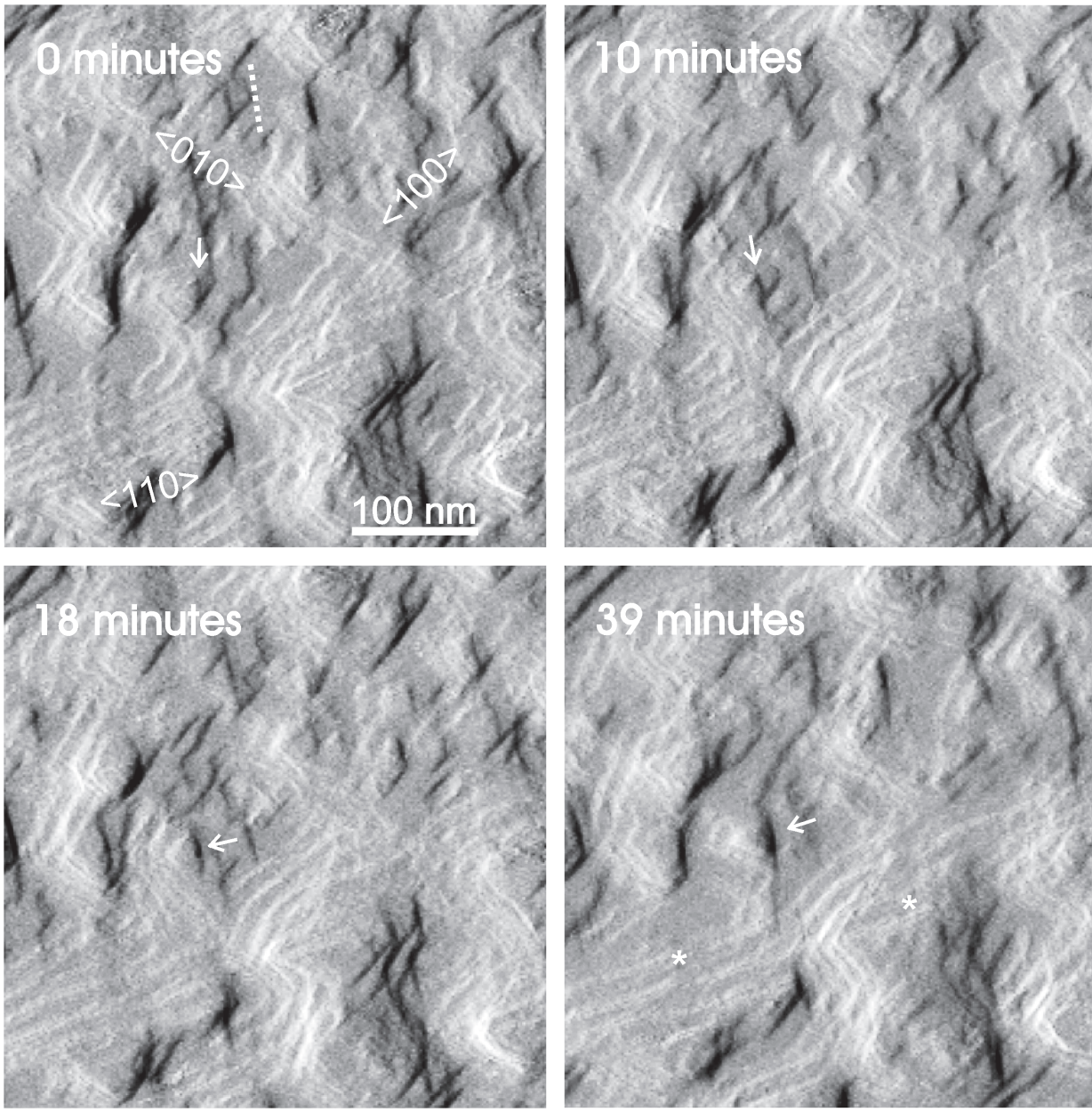

FIGURE 2. Dissolution of Russian gibbsite in 8 *M* nitric acid; AFM deflection images. The orientations of <110>, <010>, and <100> steps are shown, and the dotted line represents a non-crystallographic cleavage step direction. The arrows in the 0 and 10 minute frames point to a structure like an inverted V, with the right step higher than the left; the point of the V is the position of a screw dislocation. In the 18 and 39 minute frames, an etch pit has opened at the dislocation (arrows). In areas of no new pits (asterisks), <110>-trending steps become more prominent. A second microtip of the AFM tip has caused second images for a few of the features, and has most notably repeated the steep "elbow" structure to the lower right of the arrow in the 0 minute frame and caused the <110> steps in the area of the left asterisk in the 39 minute frame to appear double.

1960). The measured step heights were therefore one unit layer high (monolayer). The non-crystallographic cleavage steps tended not to be monolayer, and had measured heights of 2–8 unit layers (Table 1).

During dissolution, the rates of retreat of the steps were measured (15 measurements) at 0.5 to 1.8 nm per minute (average 1.2 nm per minute). No significant difference was found between the rates for the three types of steps. Step velocities were not proportional to the surface density of steps (i.e., step velocities were not lower where there were more steps per unit of surface area), so they did not indicate that surface diffusion fields for the steps overlapped during dissolution; therefore, our experiments found no evidence for surface diffusion controlling the dissolution rate.

During dissolution, the steps parallel to the 3 main crystallographic directions became longer and more continuous (i.e., offset less by short sections oriented in other directions), with parallel steps in smoother areas. The non-crystallographic cleavage steps became less prevalent, and were commonly replaced with the steps parallel to the 3 crystallographic directions. Several steps had long sections of different crystallographic orientations, so that <110> and <100> sections existed for the same step. In many cases, the <100> parts of the steps decreased in length and the <110> and <010> parts increased in length. The <110> steps appeared to be the most pronounced in the areas of no new pits (Fig. 2) and were also the longest after extensive dissolution (Table 1). Therefore, the apparent stability of the steps can be expressed: <110> > <010> > <100>. The 3 crystallographic step types can have both a similar velocity of retreat and different stabilities if the stability, and therefore velocity, difference between the steps is relatively small. Evidence for such a small difference is the fact that even the less stable <100> steps persisted as straight steps and retreated in the same areas for long periods of time, and the <110> and <010> steps formed only slowly at the expense of the <100> steps. It should be noted that other straight monolayer steps of different orientations to the main step types were observed, but they were so rare that it was not possible to assign them to particular crystallographic directions with confidence.

Although the resolution was lower for the images of the Brazilian gibbsite (Fig. 1), the changes that occurred on the {001} surface with increasing dissolution were similar to those that took place on the surface of the Russian gibbsite. Steps trending in both <110> directions became more prominent after dissolution, so the apparent stability of the steps can be expressed: <110> > <130>.

Our observations agree with those of Sweegers et al. (2002b), who observed macro-steps that were a few nanometers to a micrometer or more in height on the basal surfaces of gibbsite crystals that were grown in sodium aluminate/sodium hydroxide solutions. Sweegers et al. (2002b) found that <110> steps were the most prominent type and also observed <130> steps, although they described these as being made up of segments of other step types.

Observations of the Russian gibbsite indicated that the main mechanism of dissolution is the retreat of steps. By this mechanism, the pits formed by the initial cleavage of the sample would become smoothed out. However, we also observed the formation of etch pits, which allowed the formation of new steps on the {001} surface. In Figure 2, the arrows on the 0 and 10 minute frames point to a structure shaped like an inverted V. The step on the right side of the V was found to be twice the height of that on the left side of the V. By the 18 minute frame, a pit had formed (indicated by an arrow) and deepened to at least 1.5 nm, a distance of 3 unit layers. The deepening pit caused crystallographic steps to retreat to produce a depression of increasing diameter (arrow, 39 minute frame) bound largely by <110> and <010> steps. The initial observation of a step emerging on the surface followed by the sharp deepening of the pit to several unit layers and its widening by step retreat is consistent with pit formation at a screw dislocation emerging on the {001} surface.

TABLE 1. Characteristics of steps on the {001} face of Russian gibbsite

Direction of step	Maximum measured step lengths after at least 30 minutes of dissolution (nm)	Step heights (nm)
<100>	~130	0.36 ± 0.15 0.61 ± 0.20 0.44 ± 0.15 0.52 ± 0.15 0.62 ± 0.20
<010>	~130	0.41 ± 0.15 0.44 ± 0.15 0.64 ± 0.20 0.55 ± 0.20 0.49 ± 0.15
<110>	~250	0.56 ± 0.20 0.48 ± 0.15 0.34 ± 0.15 0.43 ± 0.15 0.45 ± 0.15
Step set between <100> and <010> steps	<50	1–4

Dissolution rates were calculated using the measured changes in size of pits of known depth and of islands of known height. The bottoms and tops of these structures appeared to be and were assumed to be flat atomically. In addition, the walls of the structures were assumed to be vertical with step fronts for the three step directions parallel to the {110}, {100} and {010} faces. A specific gravity of 2.42 g/cm^3 was used (Roth et. al. 1942). The perimeters and areas of the features were determined using the program Image SXM (Bickmore et al. 1999). The method of Rufe and Hochella (1999) was used to calculate the dissolution rate in mol/m^2·s. In this method, the pit or island of initial size is considered a particle that increases or decreases in size during the time interval. The surface area is thus taken into account, and the rate is calculated using the change in volume, ΔV, the molar volume, V_m, the surface area (SA) and the time (t): Rate = $(\Delta V / V_m)/SA(t)$. The dissolution rates were calculated using the surface area of only the edges of the pit or island (the surface area of the step fronts) at which dissolution appeared to take place. The dissolution rates were then recalculated using the total surface area—that of the step fronts and the top and bottom {001} faces of the "particle" that was used to model the pit or island in question. The calculated rates of dissolution were $1.8 - 3.6 \times 10^{-7}$ mol/m^2·s using the surface area of the step fronts, and $9.5 \times 10^{-9} - 2.3 \times 10^{-8}$ mol/m^2·s using the total surface area. No difference was observed between the dissolution rates calculated from the pits and islands.

DISCUSSION

For gibbsite to be dissolved, the Al – (OH) bonds of the predominant bridging OH groups (those bonded to two Al atoms) must be broken. For an acidic solution, it has been postulated that the protonation of terminal OH groups bonded to single Al atoms at the edges of the unit layers results in local polarization and a weakening of the bonds of the bridging OH groups (Packter and Dhillon 1969; Bloom 1983; Furrer and Stumm 1986; Bloom and Erich 1987). Our observations of the

{001} surface with monolayer steps are consistent with acid attack at these edge sites. The dissolution of gibbsite has also been shown to occur on the edges of the unit layers rather than on the basal faces in sodium hydroxide solutions (Packter and Dhillon 1974) and salicylate solutions (Molis et al. 2000).

On the {001} faces, the predominance of <110>, <010>, and <100> steps over that of straight monolayer steps of other orientations after periods of extensive dissolution is indicative of the stability of these three step types. The reason for the observed step prevalence and for the difference in stability between the three step types can be understood by considering the atomic arrangements of the steps. The gibbsite structure consists of unit layers parallel to (001) that are weakly bonded together by hydrogen bonding. For this reason, we make the assumption that edges of the $Al(OH)_3$ unit layer can be approximated as cleavage faces or crystal faces when discussing the relative stabilities of the step directions.

Figure 3 shows a ball and stick model of the $Al(OH)_3$ unit layer; dashed lines indicate bonds that have to be broken in order to produce the <110>, <010>, and <100> steps. The <110> and <010> steps can be formed by cleaving the mineral so that the cleavage direction is orthogonal to the directions between neighboring Al atoms that are bridged by two OH groups, whereas the <100> steps can be formed by cleaving the mineral so that the cleavage direction is at an oblique angle to the directions between these neighboring Al atoms. Both step types have the electrical neutrality required for crystal-face stability as outlined by Wells (1946), because either type of step can be neutral due to the presence of extra H atoms at OH groups on the edges of the structure (Hsu 1989) or due to the outermost Al atoms being coordinated to 5 rather than 6 O atoms (Fleming et al. 2000).

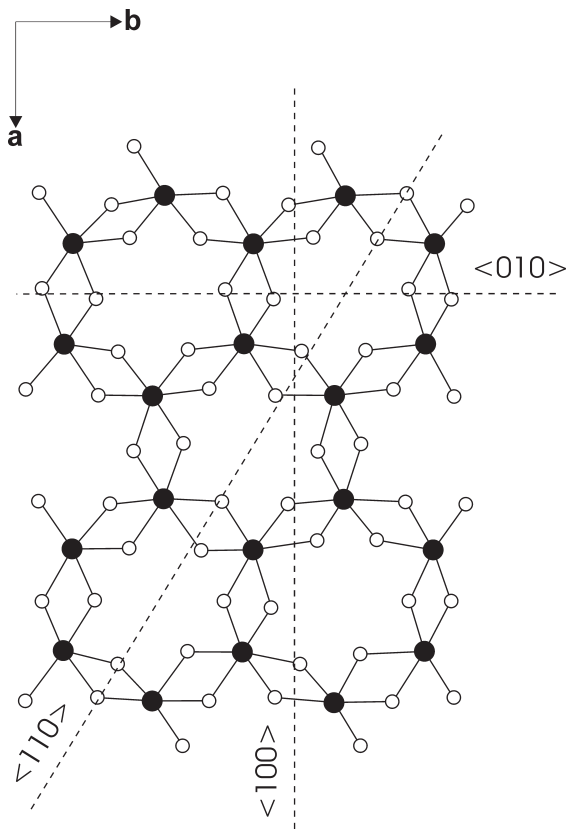

FIGURE 3. Ball and stick model of the $Al(OH)_3$ unit layer, (001) plane. Black circles represent Al atoms, white circles represent O atoms; H atoms are not indicated. Lines are indicated crossing bridging OH groups, bonds of which have to be broken in order to produce <110>, <010>, and <100> steps. A line in the <130> direction would cross the OH groups in a similar way to that for the direction <100>. Modified after Wefers and Misra (1987).

In considering the reasons for differences in stability of these steps, one can consider the cleavability of a particular surface. Huggins (1923) postulated that in cases in which all bonds are equally strong, the direction in which the mineral would be most likely to cleave would be the direction of fewest bonds, regardless of the inclination of the bonds to the direction of the cleavage. Wells (1946) showed that this was the case for many minerals. The faces formed by the breaking of the fewest bonds would also be more densely populated in terms of the ions in the surfaces.

In a similar postulate regarding what crystal faces will predominate for a given mineral, Friedel (1907) showed that the most prominent faces have the highest reticular densities, or the highest number of lattice points per unit of surface (Law of Bravais-Friedel). Therefore, the more closely packed faces would be more likely to occur. Reticular density is directly proportional to the interplanar spacing, d_{hkl}, which is the repeat distance between lattice planes parallel to the face.

The same number of bonds per unit length have to be broken to propagate <110> steps as <010> steps. Fewer bonds per unit length have to be broken to cause <110> and <010> step propagation than <100> step propagation. However, the difference in bonds per unit length is not large with the number of bridging OH groups per nm being 2.0 for the <110> and <010> step directions and 2.3 for the <100> step direction.

Figure 4 shows space-filling models of the $Al(OH)_3$ unit layer. The top edges of the models show how the layer would be truncated for: (a) a <110> or <010> step, and (b) a <100> step. The <110> or <010> step is characterized by Al atoms in a zigzag arrangement, with only every second Al atom being attached to terminal O atoms at the surface. This configuration means that none of the Al atoms attached to the terminal O atoms are attached, through O, to any other Al atoms with terminal O atoms. In this way, the additional protonation of a terminal O atom will only destabilize the bonds of one Al atom. Conversely, the <100> step is characterized by pairs of Al atoms and their terminal O atoms. It can be seen that the step is less closely packed than the <110> or <010> step, making it less stable according to Friedel (1907). In addition, each Al atom shares two of its six surrounding O atoms with the other Al atom in the pair so that the additional protonation of a terminal O atom will destabilize the bonds of two Al atoms.

It can also be seen in Figure 4 that the loss of one, or a pair of Al atoms from the <100> surface would cause a much rougher step, with more polarity, than the loss of one Al atom from a <110> or <010> step; this greater polarity in the <100> step would cause the other ions to be removed more rapidly.

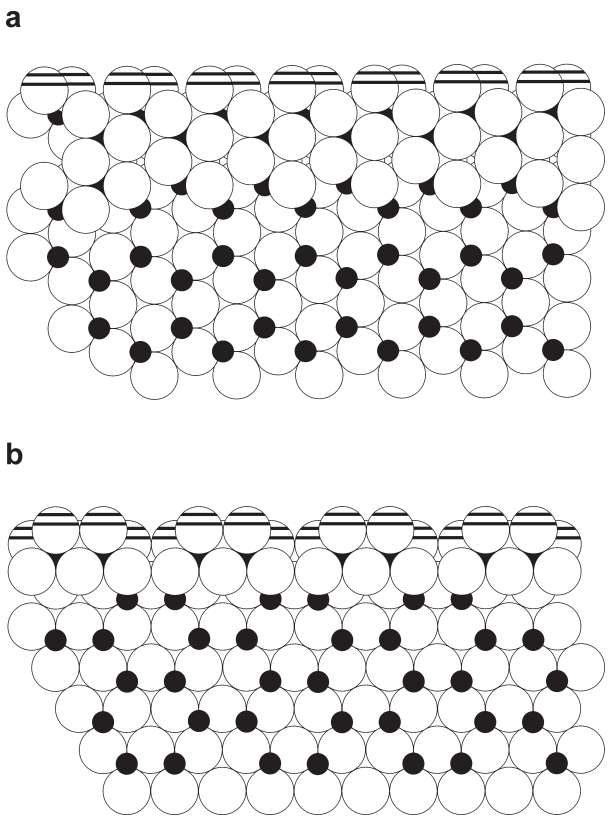

FIGURE 4. Space-filling models of the $Al(OH)_3$ unit layer, (001) plane. Black circles represent Al atoms, white circles represent O atoms, and horizontally ruled circles signify terminal O atoms that are bonded to only one Al atom; H atoms are not indicated. Top edges of models indicate how a unit layer would be truncated for: (**a**) a <110> or <010> step, and (**b**) a <100> step (these are not relaxed surface models).

The relative stabilities of different steps on the {001} face of gibbsite, as explained by consideration of step structure, are consistent with the observations made in our dissolution experiments. Because the $Al(OH)_3$ unit layers are weakly bonded together, it is likely that a similarity exists between the stability of faces other than {001} (predominantly {*hk*0} faces perpendicular to the {001} faces) and monolayer steps on the {001} faces. Therefore, we make comparisons between the relative stabilities of the monolayer steps and those of crystal faces that have crystallographic directions of those steps. The stability differences of the steps are consistent with the morphologies of gibbsite crystals. In most natural crystals, the {*hk*0} faces present are the {110} and {100} faces (which are parallel to [*hk*0] directions <110> and <010>) (Eswaran et al. 1977; Deer et al. 1992); these faces were also the {*hk*0} for the large Russian gibbsite crystals used in our study. Crystals synthesized in the Bayer Process of the aluminum industry also display {100} and {110} faces (Lee et al. 1996). The {010} faces (that are parallel to the [*hk*0] direction <100>) are only rarely observed in gibbsite (e.g., Goldschmidt 1918; Rodgers 1993), and Sweegers et al. (2002a), using a 2-dimensional growth model for gibbsite in sodium aluminate/sodium hydroxide solutions, predicted that the {010} face would not occur because the rate of 2D nucleation on that face would be too high.

Our results also suggest that the <110> steps are slightly more stable than the <010> steps. The reason could be that even for a single unit layer, the two step types are not exactly the same; Seyssiecq et al. (1999) calculated that the distances between the OH ions within the $Al(OH)_3$ unit layer are somewhat larger for the (100) face than for the (110) face. Slightly closer packing of the terminal O atoms may lead to more step stability. In another study, Sweegers et al. (1999) grew gibbsite crystals from sodium aluminate/sodium hydroxide solutions, and concluded that the {110} faces were the only {*hk*0} faces in "the basic morphology of [gibbsite]" (p. 253). They suggested that the {100} faces developed as the result of an interference effect by Na in the crystallizing solution, or twinning. Sweegers et al. thus concluded from their growth experiments that the morphological importance of the {110} faces was greater that that of the {100} faces.

Although dissolution on the {001} face of gibbsite in the far-from-equilibrium acidic conditions we studied proceeds primarily by step retreat, etch pits ultimately allow new steps to form. Etch pits have long been postulated to be an important factor in controlling the kinetics of mineral dissolution (e.g., Berner 1978). Etch pits will form during dissolution unless the amount of undersaturation of the solution with respect to the mineral is very small; for such a condition, the ΔG_r region is close to equilibrium (where ΔG_r is the difference between the Gibbs free energy of the reaction and the equilibrium value, with more negative ΔG_r values representing greater degrees of undersaturation). In the ΔG_r region close to equilibrium etch pits cannot form, and dissolution associated with dislocations takes place by the spiral mechanism, which is the reverse of the process of spiral growth described by Burton et al. (1951) (Blum and Lasaga 1987). Outside of the near-equilibrium ΔG_r region, below a certain critical bulk undersaturation, dissolution takes place by the opening of etch pits (Lasaga 1983). The latter develop through the strain mechanism of Cabrera and Levine (1956) in which hollow core formation is able to overcome the surface free-energy barrier for step formation. The near-equilibrium region corresponds to a comparatively slow dissolution rate, and the mechanism of dissolution in nature would be in the far-from-equilibrium region of ΔG_r characterized by faster dissolution through the formation of etch pits (Lee et al. 1998).

The formation of etch pits on gibbsite surfaces in undersaturated solutions was predicted by Nagy and Lasaga (1992). They demonstrated a correlation between solution undersaturation with respect to commercially prepared gibbsite for slightly acidic (pH 3) solutions at 80 °C and dissolution rates calculated from bulk dissolution experiments. For these conditions, at undersaturations near equilibrium, where $\Delta G_r >$ –0.2 kcal/mol, the rate of dissolution was extremely slow. With a small decrease in ΔG_r from –0.2 to –0.5 kcal/mol, there was a large increase in dissolution rate, followed by a leveling off of dissolution rate with lower ΔG_r values. Nagy and Lasaga (1992) believed that their observed large increase in dissolution rate represented the change in dissolution mechanism from near-equilibrium conditions in which etch pits did not form to far-

from-equilibrium conditions in which etch pits formed. Examining the dissolved gibbsite with SEM, they found no etch pits on surfaces dissolved in the near-equilibrium region of ΔG_r, but found large etch pits (on the scale of micrometers) on some {001} faces of two of the samples dissolved at lower undersaturations although the pits were only found on a few of the grains of each sample. In our study, we made observations at a much smaller scale, confirmed the presence of etch pits in far-from-equilibrium conditions, and showed their mode of formation and morphology.

The formation of etch pits can take place due to the presence of dislocations or point defects, or by unassisted hole nucleation (the formation of holes in defect-free areas of the crystal surface). These three mechanisms of etch-pit formation can have different contributions to the total dissolution rate. Other mineral dissolution studies have shown that the contribution of dislocations to the dissolution rate is greatest in natural conditions, whereas the contributions to dissolution of point defects and unassisted hole nucleation are greater in very undersaturated conditions such as in laboratory experiments or the Bayer process in the aluminum industry, because dislocations possess lower activation energy for the formation of etch pits (Blum et al. 1990; Lee et al. 1998). However, Brown (1972), having dissolved gibbsite in far-from-equilibrium (5 *M*) sodium hydroxide solutions of the type used in the aluminum industry, observed large etch pits (~300 nm wide and of similar depth) in the (001) surfaces and found no difference in the amount of pitting for crystals grown from industrial type (impure) solutions and solutions of high purity. He postulated that the presence of impurities at the surface alone could not have been responsible for the formation of etch pits and that other mechanisms, such as the opening of etch pits at dislocations, must have contributed to dissolution. Whether etch pits are formed due to dislocations, point defects, or unassisted hole nucleation, the mechanism of dissolution would be similar, with the pits characterized by the retreat of steps trending in the <100> (and crystallographically analogous <130>), <110>, and <010> directions, as was observed in our study.

The rates of dissolution of gibbsite for the pH of our study can be estimated by extrapolating the data of Bloom (1983) for the dissolution of reagent-grade gibbsite in nitric acid from pH 1.5 to 3.3 based on measurements of the amount of monomeric Al species in solution and surface areas measured by the N_2 adsorption BET (Brunauer-Emmett-Teller) method. The estimate using his data is 2×10^{-7} mol/m^2·s, which is in agreement with our values using the surface area of the step fronts only. Our calculated values using the step front surface area were about 10 times larger than those calculated using the total surface area. We make the assumption that the rate of dissolution would be similar for monolayer steps on the {001} face and for faces other than {001} (commonly {*hk*0} faces) due to the gibbsite structure, which consists of unit layers parallel to (001) that are weakly bonded together. The agreement of the data of Bloom (1983) with our values using the step front surface area rather than the total surface area can be attributed to the fact that the pits and islands in our study had very small thicknesses, corresponding to one or two $Al(OH)_3$ unit layers, relative to their areas in the {001} surface. Conversely, Bloom (1983) used very fine (200 nm to 20 µm fraction) grains consisting of thick (not platy) crystals that would have had high ratios of {*hk*0} surface area to total surface area.

The dissolution rate data as well as the observations of dissolution by step retreat in our study strongly suggest that the amount of {*hk*0} surface area and the amount of surface area of step fronts on the {001} surface determine the rate of gibbsite dissolution. In the conditions of our experiments, etch pits were important to the dissolution process only because they allowed the formation of new steps.

ACKNOWLEDGMENTS

The gibbsite sample from Brazil (M 11980) was provided by the Royal Ontario Museum. Electron microprobe analyses were carried out by Claudio Cermignani. This work was funded through NSERC research and equipment grants to G.S.H. and F.J.W.

REFERENCES CITED

Anthony, J.W., Bideaux, R.A., Bladh, K.W., and Nichols, M.C. (1997) Handbook of Mineralogy, volume 3, 549 p. Mineral Data Publishing, Tucson, Arizona.

Berner, R.A. (1978) Rate control of mineral dissolution under Earth surface conditions. American Journal of Science, 278, 1235–1252.

Bickmore, B.R., Rufe, E., Barrett, S., and Hochella, M.F. Jr. (1999) Measuring discrete feature dimensions in AFM images with Image SXM. Geological Materials Research, 1, 1–19.

Bloom, P.R. (1983) The kinetics of gibbsite dissolution in nitric acid. Soil Science Society of America Journal, 47, 164–168.

Bloom, P.R. and Erich, M.S. (1987) Effect of solution composition on the rate and mechanism of gibbsite dissolution in acidic solutions. Soil Science Society of America Journal, 51, 1131–1136.

Bloom, P.R. and Weaver, R.M. (1982) Effect of the removal of reactive surface material on the solubility of synthetic gibbsites. Clays and Clay Minerals, 30, 281–286.

Blum, A.E. and Lasaga, A.C. (1987) Monte Carlo simulations of surface reaction rate laws. In W. Stumm, Ed., Aquatic Surface Chemistry, Chemical Processes at the Particle-water Interface, p. 255–292. Wiley-Interscience, New York.

Blum, A.E., Yund, R.A., and Lasaga, A.C. (1990) The effect of dislocation density on the dissolution rate of quartz. Geochimica et Cosmochimica Acta, 54, 283–297.

Bosbach, D., Charlet, L., Bickmore, B., and Hochella M.F. Jr. (2000) The dissolution of hectorite: In-situ, real time observations using atomic force microscopy. American Mineralogist, 85, 1209–1216.

Brown, N. (1972) Crystal growth and nucleation of aluminum trihydroxide from seeded caustic aluminate solutions. Journal of Crystal Growth, 12, 39–45.

Burton, W.K., Cabrerra, N., and Frank, F.C. (1951) The growth of crystals and the equilibrium structure of their surfaces. Royal Society of London, Philosophical Transactions A, 243, 299–358.

Cabrera, N. and Levine, M.M. (1956) On the dislocation theory of evaporation of crystals. Philosophical Magazine, 1, 450–458.

Deer, W.A., Howie, R.A., and Zussman, J. (1992) An Introduction to the Rock-forming Minerals, ed. 2, 696 p. Addison Wesley Longman, Harlow, United Kingdom.

Dove, P.M. and Chermak, J.A. (1994) Mineral-water interactions: fluid cell applications of scanning force microscopy. In K.L. Nagy and A.E. Blum, Eds., CMS workshop lectures, Volume 7, Scanning Probe Microscopy of Clay Minerals, p. 140–169. The Clay Minerals Society, Boulder.

Dove, P.M. and Platt, F.M. (1996) Compatible real-time rates of mineral dissolution by Atomic Force Microscopy (AFM). Chemical Geology, 127, 331–338.

Eswaran, H., Stoops, G., and Sys, C. (1977) The micromorphology of gibbsite in soils. Journal of Soil Science, 28, 136–143.

Fleming, S., Rohl, A., Lee, M., Gale, J., and Parkinson, G. (2000) Atomistic modelling of gibbsite: surface structure and morphology. Journal of Crystal Growth, 209, 159–166.

Friedel, G. (1907) Etudes sur la loi de Bravais. Bulletin de la Societe Francaise Mineralogique, 30, 326–455.

Furrer, G. and Stumm, W. (1986) The coordination chemistry of weathering; I, Dissolution kinetics of Δ–Al_2O_3 and BeO. Geochimica et Cosmochimica Acta, 50, 1847–1860.

Ganor, J., Mogollon, J.L., and Lasaga, A.C. (1999) Kinetics of gibbsite dissolution under low ionic strength conditions. Geochimica et Cosmochimica Acta, 63, 1635–1651.

Goldschmidt, V. (1918) Atlas der Krystallformen, Taflen 4, 345 p. Karl Winters, Heidelberg.

Hind, A.R., Bhargava, S.K., and Grocott, S.C. (1999) The surface chemistry of Bayer process solids: a review. Colloids and Surfaces A: Physiochemical and Engi-

neering Aspects, 146, 359–374.
Hsu, Pa Ho (1989) Aluminum hydroxides and oxyhydroxides. In J.B Dixon and S.B Weed, Eds., Minerals in soil environments, ed. 2, p. 331–378. Soil Science Society of America, Madison, Wisconsin.
Huggins, M.L. (1923) Crystal cleavage and crystal structure. American Journal of Science, 5, 303–313.
Jordan, G., Higgins, S.R., Eggleston, C.M., Swapp, S.M., Janney, D.E., and Knauss, K.G. (1999) Acidic dissolution of plagioclase: In-situ observations by hydrothermal atomic force microscopy. Geochimica et Cosmochimica Acta, 63, 3183–3191.
Kipp, S., Lacmann, R., and Schneeweiss, M.A. (1995). Problems in temperature control performing in situ investigations with the scanning force microscope. Ultramicroscopy, 57, 333–335.
Lasaga, A.C. (1983) Kinetics of silicate dissolution. 4th International Symposium on Water-Rock Interaction, Misasa, Japan, p. 269–274. Okayama University, Misasa, Japan.
Lee, M., Rohl, A.L., Gale, J.D., Parkinson, G.M., and Lincoln, F.J. (1996) The influence of metal ion inclusion on the morphlogy of gibbsite. Chemical Engineering Research and Design, Transactions of the Institution of Chemical Engineers Part A, 74, 739–743.
Lee, M.R., Hodson, M.E., and Parsons, I. (1998). The role of intergranular microtextures and microstructures in chemical and mechanical weathering: Direct comparisons of experimentally and naturally weathered alkali feldspars. Geochimica et Cosmochimica Acta, 62, 2771–2788.
Lindsay, W.L. and Walthall, P.M. (1996) The solubility of aluminum in soils. In G. Sposito, Ed., The environmental chemistry of aluminum, ed. 2, p. 333–361. Lewis Publishers, New York.
Maurice, P.A., Hochella, M.F. Jr., Parks, G.A., Sposito, G., and Schwertmann, U. (1995) Evolution of hematite surface microtopography upon dissolution by simple organic acids. Clays and Clay Minerals, 43, 29–38.
Megaw, H.D. (1934) The crystal structure of hydrargillite $Al(OH)_3$. Zeitschrift fur Kristallographie, A87, 185–204.
Mogollon, J.L., Perez, D.A., Monaco, S. Lo, Ganor, J., and Lasaga, A.C. (1994) The effect of pH, $HClO_4$, HNO_3 and ΔG_r on the dissolution rate of natural gibbsite using column experiments. Mineralogical Magazine, 58A, 619–620.
Mogollon, J.L., Ganor, J., Soler, J.M., and Lasaga, A.C. (1996) Column experiments and the full dissolution rate law of gibbsite. American Journal of Science, 296, 729–765.
Molis, E., Barres, O., Marchand, H., Sauzeat, E., Humbert, B., and Thomas, F. (2000) Initial steps of ligand-promoted dissolution of gibbsite. Colloids and Surfaces A: Physiochemical and Engineering Aspects 163, 283–292.
Mulder, J., van Griensven, J.J.M., and van Breemen, N. (1987) Impact of acid atmospheric deposition on woodland soils in the Netherlands: III. Aluminum chemistry. Soil Science Society of America Journal 51, 1640–1645.
Nagy, K.L. and Lasaga, A.C. (1992) Dissolution and precipitation of gibbsite at 80°C and pH 3: The dependence on solution saturation state. Geochimica et Cosmochimica Acta, 56, 3093–3111.
Packter, A. and Dhillon, H.S. (1969) The heterogeneous reaction of gibbsite powder with aqueous inorganic acid solutions; kinetics and mechanism. Journal of the Chemical Society A, 252, 2588–2592.
———(1974) Studies on recrystallized aluminum hydroxide precipitates: kinetics and mechanism of dissolution by sodium hydroxide solutions. Colloid and Polymer Science, 252, 249–256.
Rodgers, K.A. (1993) Routine identification of aluminum hydroxide polymorphs with the laser Raman microprobe. Clay Minerals, 28, 85–99.
Roth, W.A., Wirths, G., and Berendt, H.Z. (1942) Beitrag zur thermochemie des aluminiums I. Zietschrift fur Electrochemie, 48, 264–267.
Rufe, E. and Hochella, M.F. Jr. (1999) Quantitative assessment of reactive surface area of phologopite during acid dissolution. Science, 285, 874–876.
Saalfeld, H. (1960) Strukturen des Hydrargillites und der Zwischenstufen beim Entwassern. Neues Jahrbuch fur Mineralogie, 95, 1–87.
Seyssiecq, I., Veesler, S., Pepe, G., and Boistelle, R. (1999) The influence of additives on the crystal habit of gibbsite. Journal of Crystal Growth, 196, 174–180.
Shindo, H. and Nozoye, H. (1993) Atomic force microscopic study of structures of cleaved surfaces of $CaSO_4$ after wet chemical etching. Surface Science, 287/288, 1030–1035.
Shiraki, R., Rock P.A., and Casey, W.H. (2000) Dissolution kinetics of calcite in 0.1 M NaCl solution at room temperature: An atomic force microscopic (AFM) study. Aquatic Geochemistry, 6, 87–108.
Sweegers, C., van Enckevort, W.J.P., Meekes, H., Bennema, P., Hiralal, I.D.K., and Rijkeboer, A. (1999) The impact of twinning on the morphology of γ-$Al(OH)_3$ crystals. Journal of Crystal Growth, 197, 244–253.
Sweegers, C., Boerrigter, S.X.M., Grimbergen, R.F.P., Meekes, H., Fleming, S., Hiralal, I.D.K., and Rijkeboer, A. (2002a) Morphology prediction of gibbsite crystals – An explanation for the lozenge-shaped growth morphology. Journal of Physical Chemistry, 106, 1004–1012.
Sweegers, C., Plomp, M., de Coninck, H.C., Meekes, H., van Enckevort, W.J.P., Hiralal, I.D.K., and Rijkeboer, A. (2002b) Surface topography of gibbsite crystals grown from aqueous sodium aluminate solutions. Applied Surface Science, 187, 218-234.
Wefers, K. and Misra, C. (1987) Oxides and hydroxides of aluminum. Alcoa Technical Paper 19, 92 p. Alcoa Laboratories.
Wells, A.F. (1946) Crystal habit and internal structure II. Philosophical Magazine, 37, 217–236.
Wesolowski, D.J. and Palmer, D.A. (1994) Aluminum speciation and equilibria in aqueous solution: V, Gibbsite solubility at 50°C and pH 3–9 in 0.1 molal NaCl solutions (a general model for aluminum speciation; analytical methods). Geochimica et Cosmochimica Acta, 58, 2947–2969.
Wesselink, L.G., Van Breemen, N., Mulder, J., and Janssen, P.H. (1996) A simple model of soil organic matter complexation to predict the solubility of aluminum in acid forest soils. European Journal of Soil Sciences, 47, 373–384.

MANUSCRIPT RECEIVED JULY 31, 2001
MANUSCRIPT ACCEPTED SEPTEMBER 17, 2002
MANUSCRIPT HANDLED BY JOHN RAKOVAN